LAND USE AND CLIMATE CHANGE CONTROLS ON RECHARGE, NORTHERN HIGH PLAINS AQUIFER, USA

A thesis submitted to the faculty of
San Francisco State University
In partial fulfillment of
The requirement for
The degree

Master of Science
In
Geosciences

by

Zachary Howard Lauffenburger

San Francisco, California

August 2013

CERTIFICATION OF APPROVAL

I certify that I have read Land Use and Climate Change Controls on Recharge, Northern High Plains Aquifer, USA by Zachary Howard Lauffenburger, and that in my opinion this work meets the criteria for approving a thesis submitted in partial fulfillment of the requirements for the degree: Master of Science in Geosciences at San Francisco State University.

Jason J. Gurdak
Assistant Professor of Geosciences

Leonard Sklar
Associate Professor of Geosciences

Karen Grove
Professor of Geosciences

LAND USE AND CLIMATE CHANGE CONTROLS ON RECHARGE, NORTHERN HIGH PLAINS AQUIFER, USA

Zachary Howard Lauffenburger
San Francisco State University
2013

Understanding the controls of land use/land cover and climate change on diffuse recharge rates is critically important to develop appropriate management and sustainability plans for groundwater resources, particularly those in semiarid and arid regions. Much of the High Plains study area has been converted from natural rangeland to irrigated cropland cover. Field-based recharge rate estimates were implemented to quantify the differences in recharge rates beneath two rangeland and two irrigated corn sites along an east-west transect in the Platte River Basin in central Nebraska. Historical climate data and the field-based estimates were used to calibrate HYDRUS-1D computer models. A total of 16 different global climate models (GCMs) and two global warming scenarios were used to project a 2050 climate relative to the baseline 1990 climate. The low-global-warming scenario (+1.0°C) projected no statistical differences between any future variables compared to the baseline variables. The high-global-warming scenario (+2.4°C) projected up to a 98% decrease in median annual recharge rate, and a 25% and 15% increase in median annual ET and irrigation, respectively. The high-global-warming scenario projections result in a bidirectional shift of climate gradients. Future northern High Plains temperatures will resemble current central High Plains temperatures and future recharge rates at the eastern study sites will resemble current recharge rates at the western study sites.

I certify that the Abstract is a correct representation of the content of this thesis.

Chair, Thesis Committee

7-22-2013

Date

ACKNOWLEDGMENTS

I would like to thank Jason Gurdak for his wonderful guidance throughout my time at San Francisco State University. He helped me excel in my classes, teaching and research. I truly cannot thank him enough. I would also like to acknowledge my committee members Karen Grove and Leonard Sklar for their patience and unwavering optimism. Special thanks go to Ryan Corbett and to my family and friends who believed in me from start to finish.

Partial funding for this research was provided by the Nebraska Department of Natural Resources Interrelated Water Management Funds. I thank the cooperation of the land owners who graciously provided access to their land, the Central Platte Natural Resources District, especially Duane Woodward for assistance with the installation, monitoring, and maintenance of the field sites, and U.S. Geological Survey (USGS) Hydrologists Greg Steele and Chris Hobza for their assistance with providing historical recharge estimates.

Finally, I'd like to thank Russell Crosbie for providing me with all the downscaled global climate model data. Without him, I'd still be trying to determine the direction of my project. Even living on the other side of the planet, he gave timely and insightful comments that helped me understand the complexities of downscaling and global climate models.

TABLE OF CONTENTS

LIST OF TABLES

LIST OF FIGURES

Fig. 5: Simulated historical (1990) and future (2050) (a,c) average annual recharge (mm yr–1) and (b,d) percent (%) change in average annual recharge at the western and eastern study area sites beneath (a, c) rangeland and (b, d) irrigated corn for low (+1.0°C, 478 ppm CO2) and high (+2.4°C, 567 ppm CO2) global warming scenarios. Each boxplot represents the median of 30 years of simulated average annual recharge from 16 global climate models (GCMs). The field-based recharge estimates from tritum (3H), chloride-mass balance (CMB), applied potassium bromide trace (KBr), and groundwater-age dating (GW) methods are listed in Table 3.

LIST OF APPENDICES

App. 3: Boxplots of the percent (%) change in simulated average annual evapotranspiration between 2050 and 1990 at Gothenburg, Nebraska (western study area) and Grand Island, Nebraska (eastern study area) for (a) high global warming scenario (+2.4°C, 567 ppm CO2) and (b) low global warming scenario (+1.0°C, 478 ppm CO2) from 16 global climate models (GCMs). Each boxplot represents 30 years of simulated precipitation. The dashed line represents no change; positive values indicate greater future average annual precipitation and negative values indicate smaller future average annual precipitation. Note the different y-axis scales.

App 4: Boxplots of the percent (%) change in simulated average annual recharge between 2050 and 1990 at the western and eastern study area sites beneath (a,c) rangeland and (b,d) irrigated corn for (a,b) high global warming scenario (+2.4°C, 567 ppm CO2) and (c,d) low global warming scenario (+1.0°C, 478 ppm CO2) from 16 global climate models (GCMs). Each boxplot represents 30 years of simulated recharge. The dashed line represents no change; positive values indicate greater future average annual precipitation and negative values indicate smaller future average annual precipitation. Note the different y-axis scales for (c) rangeland (low scenario).

1.0 Introduction

Accurate estimates of diffuse recharge under gradients of land use/land cover (LULC) and historical and future climate are needed to develop well-constrained groundwater budgets and conjunctive use strategies with the goal of maintaining sustainable groundwater resources (Hanson et al. 2012). Groundwater resources are replenished primarily by diffuse, rain- and irrigation-fed recharge and focused recharge via ephemeral streams, wetlands, or lakes (Taylor et al. 2012). At the aquifer scale, because diffuse recharge occurs fairly uniformly over large areas, it is generally a larger fraction of the inflow to the groundwater budget than focused recharge (Scanlon et al. 2002). At the global scale, estimates of diffuse recharge rates range from 13,000 to 15,000 $km^3\ yr^{-1}$ (Döll and Fiedler 2008; Wada et al. 2010). This amount is about 30% of the world's renewable freshwater resources and works out to a mean per capita groundwater recharge rate of 2,100 to 2,500 $m^3\ yr^{-1}$ (Döll 2009).

Climate variability and change will likely cause significant changes to the spatiotemporal patterns of diffuse recharge (Green et al. 2011). Döll (2009) estimated that by the year 2050, approximately 18% of the global population could be affected by water shortages, with decreased recharge of at least 10%; on the other hand, approximately 20–33% of the global population could be affected by flooding hazards, with increased recharge of at least 10%. The high socioeconomic value of diffuse recharge, coupled with the uncertainty surrounding future LULC and climate variability and change, is driving many management concerns and scientific questions about current and future diffuse recharge and the implications for renewable groundwater resources (Döll 2009; Green et al. 2011; Taylor et al. 2012).

The rates and timing of diffuse recharge are largely a function of the locally prevailing LULC, historic and future climate (precipitation plus irrigation minus evapotranspiration (ET)), and hydraulic and geologic properties of the vadose zone. Arguably, the most profound effect on diffuse recharge rates has been the historical conversion of natural rangeland and perennial vegetation to irrigated agriculture (Taylor et al. 2012). In some regions, recharge rates beneath irrigated cropland have been reported to be 1–2 or more orders of magnitude greater than recharge rates beneath adjacent natural rangeland (McMahon et al. 2006; Scanlon et al. 2005; 2006). In a synthesis of the literature, Taylor et al. (2012) concluded that LULC may actually have a stronger effect on the hydrology than climate change, including the potential effects on diffuse recharge.

Climate variability and change manifest as local-scale spatiotemporal patterns in precipitation and ET that drive diffuse recharge dynamics. Many studies have predicted reduced recharge rates under future climate (Earman and Dettinger 2011; Green et al. 2011), however the effects of climate change on recharge might not be negative in all aquifers during all time periods (Döll 2009; Green et al. 2011). Dettinger and Earman (2007) concluded that it is unknown whether the overall response of recharge to climate change will increase, decrease, or stay the same at any scale in the western United States

(U.S.). Some studies have demonstrated that small changes in precipitation could amplify changes to recharge (Green et al. 2011; Woldeamlak et al. 2007). For example, Sandstrom's (1995) conceptual model was developed and applied to a catchment in semiarid Tanzania. The simulated climate change scenario showed that a 15% reduction in precipitation, with no change in air temperature, resulted in a 40–50% reduction in recharge (Sandstrom 1995).

The vadose zone, particularly in semiarid and arid regions, has slowly evolving, dynamic characteristics that pose considerable challenges in efforts to quantify the spatiotemporal pattern of diffuse recharge and understand the temporal lags between LULC and climate change and corresponding diffuse recharge dynamics (Green et al. 2011; Gurdak et al. 2007; Phillips 1994). The hydrodynamic responses in the vadose zone to climate variability and change are not well understood largely because of a general lack of field observations throughout the entire vadose zone and over time scales longer than one to two years (Gurdak et al. 2007). Without field observations to calibrate unsaturated flow models and verify model results, approaches such as numerical modeling experiments, sensitivity analyses, and stochastic parameterization of climate forcings have been used to estimate diffuse recharge (Carrera-Hernández et al. 2012; Small 2005).

Accurately estimating historic (baseline conditions) and future diffuse recharge is largely motivated by the need to better manage local- to regional-scale groundwater resources, particularly in those aquifers in semiarid and arid regions that have unsustainable rates of groundwater abstractions. The High Plains aquifer in the central U.S. (Fig. 1) is among the most internationally recognized examples of unsustainable groundwater abstraction (Gurdak et al. 2012; Scanlon et al. 2005; Sophocleous 2012; Taylor et al., 2012). Although the High Plains aquifer has been studied extensively (Crosbie et al. 2013; McMahon et al. 2007; Gurdak et al. 2009; 2012; Scanlon et al. 2012), many questions remain about the effects of LULC, climate gradients, and future climate change on diffuse recharge. In response, the United States Geological Survey (USGS) established the regional and field-based High Plains Unsaturated-Zone Research Network (HPUZRN) (Fig. 1) to more accurately determine the controls on the rates and quality of recharge (Gurdak et al. 2007; 2009; McMahon et al. 2003; 2006; 2007; Steele et al. in review).

This thesis presents a field- and modeling-based investigation of the atmospheric and subsurface variables that influence diffuse recharge rates in the northern High Plains aquifer beneath two irrigated cropland and two natural rangeland sites in the USGS HPUZRN along an east-west precipitation gradient in the Platte River Basin of central Nebraska. First, recharge rates were estimated using physical, chemical, and HYDRUS-1D (Šimůnek et al. 2008) modeling methods beneath the four sites. Second, the calibrated HYDRUS-1D models and climate output from 16 global climate models (GCMs) were used to simulate historical (1990) and future (2050) diffuse recharge rates at the four sites under two CO_2 emission and warming scenarios from the Special Report on Emission Scenarios (SRES) (IPCC 2007).

The objectives of this investigation are to use field-based recharge rate estimates to; first, better understand the effects of LULC on the quantity of water that recharges the aquifer and second, better understand the effect the east-west precipitation gradient across Nebraska has on recharge rates. The third research objective is to use 16 different GCMs and two global warming scenarios to project changes in precipitation, irrigation demands, evapotranspiration (ET), and recharge rates at the four field sites for a 2050 climate relative to a 1990 climate. The final research objective is to discuss how water managers should plan for a future under projected climate change scenarios. Based on previous studies (McMahon et al. 2006; Scanlon et al. 2005; 2006; Taylor et al. 2012), it is hypothesized that irrigated sites will have higher recharge rates than the adjacent rangeland sites in response to irrigation return flow into the subsurface. In addition, based on previous studies (Crosbie et al. 2013; Szilagyi et al. 2001), it is hypothesized that the eastern study sites will have higher recharge rates in response to higher average annual precipitation compared to western study sites. This is the first study of the High Plains aquifer to use field-calibrated unsaturated flow models to simulate historical and future diffuse recharge while considering the effects of climate change at the spatial scale that is consistent with groundwater management and planning in the High Plains.

2.0 Study Area

The High Plains aquifer, also known locally as the Ogallala aquifer, spans 450,000 square kilometers (km^2) in the Great Plains physiographic province and underlies parts of eight states (Colorado, Kansas, Nebraska, New Mexico, Oklahoma, South Dakota, Texas, and Wyoming) (Fig. 1). The High Plains aquifer is often subdivided into three aquifers because there is little hydraulic connection between the northern, central, and southern High Plains aquifers (Gurdak et al. 2008) (Fig. 1). The High Plains aquifer is composed of extensive unconsolidated to semi-consolidated Neogene- to Quaternary-aged clay, silt, sand, and gravel with scattered zones cemented by calcium carbonate (Maupin and Barber 2005; McGuire et al. 2003; McMahon et al. 2006). The depth to groundwater is 15–40 meters (m) under natural rangeland and 25–60 m under irrigated cropland (McMahon et al. 2006). Wind-blown silt and sand have created a topography of flat to gentle slopes overlain by coarse-textured soils that allow moderate to high infiltration rates (McMahon et al. 2006).

The High Plains region is characterized by a middle-latitude dry continental climate (Gutentag et al. 1984). The large areal extent of the High Plains results in relatively large north-to-south gradients in mean annual air temperature (6–17°C) and east-to-west gradients in mean annual precipitation (711–406 millimeters (mm)) (Fig. 1). Abundant sunshine, frequent winds, and low humidity generate high rates of evaporation (Dennehy et al. 2002; Gurdak et al. 2007; Gutentag et al. 1984; McMahon et al. 2006).

The High Plains aquifer has the greatest annual groundwater withdrawal of the 62 U.S. principal aquifers, which are regionally extensive aquifers of national significance because they are critically important sources of potable water (Maupin and Barber 2005). Starting in the late 1940s, large-scale irrigation began in the High Plains region (McMahon et al. 2006; Qi et al. 2002). In 2000, almost 97% (640 million cubic meters per day (Mm^3 day^{-1})) of the total withdrawals (660 Mm^3 day^{-1}) were used for irrigation (Maupin and Barber 2005). The water pumped from the aquifer is used to irrigate crops on about 27% of the irrigated land in the U.S. (Dennehy et al. 2002), and groundwater withdrawals account for about 30% of the Nation's groundwater used for irrigation (Maupin and Barber 2005). Agriculture accounts for 94% of the water use and supports nearly 20% of the wheat, corn, cotton, and cattle produced in the U.S. (Kromm and White 1992). Drinking water accounts for about 2% (1.5 Mm^3 day^{-1}) of the water pumped from the aquifer (Maupin and Barber 2005), which provides water for over 80% of the residents who live within the aquifer boundary (Dennehy et al. 2002).

The four study sites (Table 1; Fig. 1) are located in the Central Platte Natural Resource District (CPNRD) that helps to protect and manage groundwater and other natural resources. The eastern rangeland (ER) and eastern irrigated corn (EIC) sites are northwest of Grand Island, Nebraska, and the western rangeland (WR) and western irrigated corn (WIC) sites are northeast of Gothenburg, Nebraska (Table 1; Fig. 1). Historical records show that, on average, more precipitation falls near Grand Island (622 mm yr^{-1}, 1962 to 2009) than near Gothenburg (557 mm yr^{-1}, 1895 to 2010) (National Oceanic and Atmospheric Administration 2013a). From 1939 to 2009, average monthly temperatures in Grand Island ranged from –5.0°C in January to 24.9°C in July; from 1895 to 2010, average monthly temperatures in Gothenburg ranged from –3.7 °C in January to 24.3°C in July (National Oceanic and Atmospheric Administration 2013a). The CPNRD is within the study area of the Platte River Cooperative Hydrology Study

(COHYST) that assists the State of Nebraska in meeting the Three-State Cooperative Agreement (Luckey and Cannia 2006). Colorado, Nebraska, Wyoming, and the U.S. Department of the Interior (DOI) entered into the Three-State Agreement in 1997 to maintain critical flows in the Platte River for endangered and threatened species, assist Natural Resources Districts (NRDs) with regulation and management of groundwater, and provide Nebraska a basis for establishing and implementing groundwater and surface-water policy and procedures (Steele et al. in review).

3.0 Methods

3.1 Vadose zone monitoring sites

Between 2008 and 2010, four vadose zone monitoring sites were installed and instrumented following methods outlined by McMahon et al. (2003; 2006) and Gurdak et al. (2007). The four sites have a similar design and capability as the nine existing sites in the HPUZRN that aims to assess the processes and rates of water movement, including diffuse recharge rates, and storage and transit times of chemicals in the vadose zone (Gurdak et al. 2009; McMahon et al. 2007). Details about the installation, sample collection and analysis, and capabilities of the four sites are described by Steele et al. (in review), and summarized below.

At each site a single 15-cm borehole was drilled to the water table using a hollow-stem auger (Steele et al. in review). During drilling, continuous core samples of the vadose zone were collected using a split-spoon core barrel to collect samples for lithologic descriptions. Each core was cut into five equal subsections for laboratory analysis of physical and chemical properties of the sediment and pore water. One subsection of core was analyzed by the U.S. Department of Agriculture (USDA) Natural Resources Conservation Service (NRCS) National Soils Survey Laboratory (NSSL) in Lincoln, Nebraska for soil particle-size [L], bulk density (ρ_b) [M L^{-3}], and water content (θ) [L^3 L^{-3}] using the NRCS classification and standard procedures (Soil Survey Staff, 1999). A second subsection of core was analyzed by the USGS Tritium Laboratory in Menlo Park, California, for tritium (^3H) in pore water using vacuum distillation; concentrations were quantified by electrolytic enrichment and liquid scintillation counting (Thatcher et al. 1977). The 1-sigma precision of the analysis ranged from 0.3 to 2.8 tritium units (TU) and was better for moist sediment cuttings than for dry ones (Steele et al. in review). A third subsection of core was analyzed at the San Francisco State University (SFSU) Hydrogeology Laboratory for water-extractable concentrations of bromide (Br^-), chloride (Cl^-), and nitrate (NO_3^-) using ion chromatography (Dionex ICS-900 model), with a detection limit of 0.2 micrograms per gram ($\mu g\ g^{-1}$) and following methods described by Herbel and Spalding (1993), Lindau and Spalding (1984), and McMahon et al. (2003). The remaining subsections of core were sealed and archived.

Heat dissipation probes (HDPs) were installed in the borehole using methods consistent with McMahon et al. (2006) and Gurdak et al. (2007) and at depths of major lithologic units in the vadose zone (Steele et al. in review). HDPs measure real-time matric potential (ψ_m) values between approximately –0.01 to –100 megapascals (MPa) (Flint et al. 2002). Total water potential (ψ_T) values were calculated as the sum of ψ_m and gravitational potential (ψ_g), which assumes that the thermal and osmotic potentials are negligible (Gurdak et al. 2007; McMahon et al. 2006). The borehole was completed with steel surface casing and cement pad to help prevent borehole leakage. Each site was installed with three, vertically-nested monitoring wells with short screens (1.53 m) to determine vertical gradients in groundwater chemistry and age to help estimate recharge rates. Further details about well construction and groundwater sampling are provided in Steele et al. (in review).

A potassium bromide (KBr) solution was applied to the land surface as a conservative tracer at all four sites. Approximately 278 g/L of KBr and de-ionized water mixture was applied evenly to each 1 m^2 grid plots at the ER and EIC sites in May 2009. Approximately 100 g/L of KBr mixture was applied evenly to each 1 m^2 grid plots at the WR and WIC sites in June 2010. Continuous cores were collected at all four sites in April 2012 to determine the infiltration depths of the Br^- in pore water from the KBr tracer. The water-extractable concentrations of Br^- in the core were analyzed at the SFSU Hydrogeology Laboratory using ion chromatography, as previously described.

3.2 Recharge methods

The physical and chemical data from the four vadose zone monitoring sites were used in a number of methods to evaluate water movement through the vadose zone and to estimate diffuse recharge rates at the sites. Diffuse recharge rates were estimated by (i) standard peak-displacement and mass-balance methods for the ^3H, Cl^-, and Br^- tracer data (Allison and Hughes 1978; Healy 2010; McMahon et al. 2003) and (ii) groundwater-dating methods using atmospheric environmental tracers (chlorofluorocarbons (CFCs-12, -11, and -13), sulfur hexafluoride (SF_6), ^3H, and tritium/helium ($^3H/^3He$)) (Delin et al. 2000; 2007). HDP time series of ψ_T (ψ_m plus ψ_g) for selected depths below land surface indicated relatively sharp- and uniform-wetting fronts, similar to ψ_T profiles seen at the other HPUZRN sites (Gurdak et al. 2007). The HDP ψ_T profiles were used to qualitatively verify the wetting fronts simulated by HYDRUS-1D. All recharge methods, sampling procedures, and laboratory analytical methods are detailed by Steele et al. (in review) and are consistent with the methods used by Gurdak et al. (2007) and McMahon et al. (2006) at the HPUZRN sites.

3.3 Recharge modeling

Site specific HYDRUS-1D numerical models (Ŝimůnek et al. 2008) were built to simulate diffuse recharge rates under a projected 2050 climate relative to diffuse recharge rates under historical climate defined for the year 1990. HYDRUS-1D solves Richards' equation (Richards 1931) for saturated and unsaturated water flow in one-dimension and the advection-dispersion equation for solute transport (Ŝimůnek et al. 2008). The site-specific HYDRUS-1D numerical models were calibrated using data from the vadose zone monitoring sites, including soil texture and ρ_b, ψ_T, and water content (θ). The historical recharge rates simulated with HYDRUS-1D were verified using the field-based diffuse recharge estimates.

Soil textures in the HYDRUS-1D models were based on the USDA NRCS NSSL soil textural analyses, and corresponding hydraulic properties were defined using the

Rosetta Dynamically Linked Library in HYDRUS-1D (Schaap et al. 2001). Rosetta uses pedotransfer functions (PTFs) to estimate van Genuchten (1980) water retention parameters and the saturated hydraulic conductivity (K_S) in a hierarchical manner from soil textural class information, the soil textural distribution, ρ_b, using one or two water retention points as input (Schaap et al. 2001).

The HYDRUS-1D model domains were bounded at the top by transient atmospheric boundary conditions assuming surface run off and at the bottom by a zero-gradient boundary condition to simulate freely draining soil profiles. Thus, the water flux across the lower boundary simulates diffuse recharge. The transient boundary conditions were based on daily time steps with six variables: precipitation, solar radiation, maximum and minimum temperature, relative humidity, and wind speed. The six variables are described in detail in section 3.4. HYDRUS-1D calculates potential ET using the Penman-Monteith combination equation (Monteith 1981; Monteith and Unsworth 1990).

The HYDRUS-1D models simulated root-water uptake using parameters defined by Feddes et al. (1978), with specific values for either pasture (sites ER and WR) or corn (sites EIR and WIR) based on studies by Wesseling et al. (1991). The rangeland (ER and WR) sites are characterized by mixed-grass prairie plant species, including tall and short rhizomatous and bunchgrasses, and many forbs (University of Nebraska-Lincoln 2010). Rangeland sites crop height (2 m) and rooting depth (2.5 m) were averaged from root systems of prairie plants (Conservation Research Institute 1995). Maximum crop height (2 m) and rooting depth (1.7 m) in irrigated corn (EIR and WIR) sites were defined based on the Food and Agriculture Organization (FAO) of the United Nations (1998). Corn stalk and root growth were assumed to be linear over the growing season that extends from late June through early September.

As an additional HYDRUS-1D calibration constraint, a conservative solute was simulated and resulting fluxes and transit depths in the vadose zone were compared to observed fluxes and depths of the applied KBr tracer at each site. The top of each model domain was a concentration flux boundary condition that allowed the initial infiltrating water to simulate a conservative solute concentration similar to the applied KBr tracer concentration. The bottom of each model domain was initially bounded by a zero-concentration gradient.

3.4 Historical and future climate data

A 30 year (1981–2011) historical climate data set from the National Oceanic and Atmospheric Administration (NOAA) National Climate Data Center (NCDC) (http://www.ncdc.noaa.gov/) defined the time-variable boundary conditions in the historical (1990) HYDRUS-1D models. The historical climate data was used to calculate saturation vapor pressure (*SVP*) (kPa) as:

$$SVP = 0.618e^{\frac{17.27*Tavg}{237.2+Tavg}} \qquad \text{[Eq. 1]}$$

where T_{avg} is average daily temperature (^{o}C) (Hendriks 2010). Relative humidity (*RH*) (%) was calculated as:

$$RH = \left(1 - \frac{VPD}{SVP}\right) * 100\% \qquad \text{[Eq. 2]}$$

where *VPD* is vapor pressure deficit (kPa) (Crosbie et al. 2013; Wanielista et al. 1997). Solar radiation data were obtained from the National Center for Atmospheric Research (NCAR)/National Centers for Environmental Prediction (NCEP) (Crosbie et al. 2013; Kalnay et al. 1996). The wind speed data are historical 10 m wind speeds obtained from daily 1/8-degree gridded meteorological data (Maurer et al. 2002). Historical wind speed data were used for all historical and future HYDRUS-1D models because future wind speed is not simulated by the GCMs.

The historical 30 year (1981–2011) climate is assumed to be a baseline and representative of a 1990 climate, an approach that is consistent with recent climate-impact studies (Crosbie et al. 2011; 2013). The 30 year climate time series was run in HYDRUS-1D as a model spin-up to establish the initial conditions of the unsaturated flow models. The spin-up model output data for θ and soil temperature at each grid spacing were input into HYDRUS-1D as initial profile conditions, and the 30 year climate data were re-run to simulate the historical (1990) ET and recharge.

Because the overall objective of the modeling was to investigate the effects of a projected 2050 climate, relative to a 1990 climate, on diffuse recharge rates, a constant atmospheric CO_2 concentration was used rather than a time series. The observed atmospheric CO_2 concentration in 1990 was 353 ppm (IPCC 2007), which was assumed to be constant for the historical baseline period. Two future global warming scenarios were used to simulate 2050 conditions: low global warming (478 ppm CO_2 and an increase of 1.0°C) and high global warming (567 ppm CO_2 and an increase of 2.4°C). The atmospheric CO_2 concentrations and associated temperature changes for the low and high warming scenarios were inferred from the IPCC (2007) to represent the range of SRES scenarios (Nakicenovic and Swart 2000). A total of 16 different GCMs were used to model each scenario (Table 2), thus incorporating as much uncertainty as possible into the projections (Crosbie et al. 2011; Holman et al. 2012). Daily data for the 16 GCMs were obtained from the World Climate Research Programme's Coupled Model Intercomparison Project phase 3 (CMIP3) multi-model dataset (Crosbie et al. 2013; Meehl et al. 2007).

Following the approach of Crosbie et al. (2011; 2013), the daily scaling method (Chiew et al. 2009) was used to spatially downscale daily time series (precipitation, temperature, VPD, and solar radiation) from the GCM grid scale to the point scale for use in the HYDRUS-1D models. Many GCMs indicate that future extreme high precipitation is likely to be more intense, even in some regions where a decrease in mean seasonal or annual precipitation is projected (Chiew et al. 2009). The Chiew et al. (2009) method created future temporal sequencing of precipitation similar to historical precipitation, but scales changes in daily precipitation intensity (Crosbie et al. 2013).

Irrigation requirements for corn were estimated from CROPSIM, a computer simulation model developed at the University of Nebraska-Lincoln by Dr. Derrel Martin (Nebraska Department of Natural Resources 2010). The difference between ET and effective precipitation were plotted against net irrigation for the CROPSIM Grand Island (eastern study area) (r^2=0.76) and Gothenburg (western study area) (r^2=0.77) models. The polynomial regression equations for the eastern and western study area were used to estimate irrigation requirements for the historical and future EIC and WIC HYDRUS-1D models. Simulated irrigation was not applied to the ER or WR HYDRUS-1D models.

The water balance within the model domain consists of five variables for the rangeland site models and six variables for the irrigated corn site models. Initial water contents are established within the soil profiles before the models are run. During the model run, precipitation and irrigation water (for irrigated corn sites only) enter the model domain, and ET, surface runoff, and recharge water exit the model domain. At the conclusion of the model run there is still water held in storage within the soil profiles.

4.0 Results

4.1 Field-based estimates of diffuse recharge rates

Diffuse recharge rates that were estimated from the ^3H, Cl^- mass-balance (CMB), KBr tracers, apparent groundwater ages, and simulated conservative tracer from the HYDRUS-1D models are shown in Table 3. As expected, site-specific recharge estimates vary somewhat by method (Table 3) because of the inherent uncertainties and different spatial and temporal support scales for each method (Scanlon et al. 2002). In general, the recharge rates estimated from the KBr tracer are greater than those estimated from the ^3H, CMB, or apparent groundwater ages, because the KBr tracer represents infiltration rates and near-surface fluxes that have responded to transient atmospheric conditions since the KBr was applied in 2009. The recharge estimated from the ^3H, CMB, and apparent groundwater ages are more representative of water flux and recharge rates at the sites over long-term (decadal) time scales. Diffuse recharge rates were not estimated at some sites because of flushing of postbomb ^{3}H (sites ER and WIC), uncertainties associated with Cl^{-} concentrations in applied irrigation water (sites WIC and EIC), and (or) the apparent ages are older than the groundwater dating methods used in this study (site EIC) (Table 3) (Steele et al. in review).

Results indicate that spatial patterns in diffuse recharge are controlled primarily by LULC and to a lesser extent by average annual west-east (low to high) precipitation gradients. The recharge rates are generally greater beneath the irrigated corn sites EIC and WIC (59–218 mm yr^{-1}) than the rangeland sites ER and WR (1–201 mm yr^{-1}), which is a spatial pattern consistent with findings from previous recharge studies in the High Plains (McMahon et al. 2006; Scanlon et al. 2005). Irrigation return flow, or irrigation water that infiltrates below the root zone, likely contributes to the greater recharge rates beneath irrigated fields. Differences in recharge rates beneath western and eastern sites are less apparent, in part, because recharge could not be estimated using all methods beneath all sites, as previously discussed. However, the available estimates indicate somewhat greater recharge rates beneath eastern sites than western sites for most methods. The CMB method indicates greater recharge rates beneath ER (mean, 21 mm yr^{-1}) than WR (mean, 13 mm yr^{-1}) (Table 3). The KBr method indicates greater recharge rates beneath ER (center of mass, 38 mm yr^{-1}) than WR (center of mass, 35 mm yr^{-1}) and greater recharge rates beneath EIC (center of mass, 207 mm yr^{-1}) than WIC (center of mass, 65 mm yr^{-1}) (Table 3). However, the groundwater-dating method indicates greater recharge rates beneath WR (mean, 34 mm yr^{-1}) than ER (mean, 24 mm yr^{-1}). The groundwater-dating methods inherently integrates recharge over a much larger spatial extent than the vadose-zone based ^{3}H, CMB, and KBr tracer estimates of recharge, and thus may not accurately represent site-specific conditions beneath WR and ER. As discussed below, the general west-east increasing trend in recharge rates could be a response to the west-east increasing trend in average annual precipitation, which is also a finding that is consistent with some previous studies (Crosbie et al. 2013; Szilagyi et al. 2001).

4.2 Modeled estimates of historical diffuse recharge rates

Statistical analyses included the Wilcoxon signed-rank test to determine whether the median difference between paired observations equals zero. Tables 4–7 list p-values for each paired comparison. Where the p-value is less than alpha-value of 0.05 (95% confidence level), the median values are statistically different. The 30-year median of historical (1990) total annual precipitation in the western and eastern study areas is not statistically different (p-value = 0.16) (Table 4) even though the eastern study area has a substantially greater range in total annual precipitation (white boxes in Fig. 2a). The simulated 30-year median of historical (1990) annual irrigation (mm yr^{-1}) (Fig. 3a) and annual ET (mm yr^{-1}) in the rangeland sites (Fig. 4a) is statistically different (p-values = < 0.001 and 0.007, respectively) (Table 5) between the western and eastern study areas. The sites in the western study area have substantially greater irrigation (Fig. 3a) and ET (Fig. 4a) than corresponding sites in the eastern study area. Although the median ET values are not statistically different (p-value = 0.959) (Table 6) between the two irrigated corn sites (WIC and EIC) (Fig. 4b), the median ET values are statistically different between the paired irrigated and rangeland sites in the western (WIC and WR, p-value < 0.001) and eastern (EIC and ER, p-value < 0.001) study area (Table 6). In both cases, the median ET is greater at the irrigated corn sites (Fig. 4ab).

The input of historical precipitation, irrigation, and ET resulted in simulated near-surface water and solute fluxes, and diffuse recharge rates that compare reasonably well with the respective KBr tracer (Table 3) and other field-based recharge estimates (Fig. 5a,b). The HYDRUS-1D simulated tracer fluxes from the center of mass and peak displacement methods (Table 3) were calculated at three time steps (498, 996 and 1,494 days, not shown in Table 3) to correspond with the approximate time since the application and sampling of the KBr tracer at the sites. In general, the simulated tracer tends to overestimate actual KBr tracer fluxes, except at the EIC and WR sites that respectively match and somewhat underestimate the KBr tracer fluxes. The simulated historical recharge rates (Fig. 5a, b) compare reasonably well with the field-based recharge rates (Table 3); the field-based recharge rates either overlap (sites WR, WIC, and EIC) or slightly underestimate (sites ER) the simulated distribution of recharge rates. The consistency of the simulated near-surface water flux and recharge rates with the field-based near-surface water flux and recharge rates indicates that the HYDRUS-1D models have reasonably good predictive ability in estimating historical water fluxes in the near surface and diffuse recharge rates.

4.2 Future climate projections

Output from the GCMs generally indicates greater average annual precipitation for 2050 relative to 1990 across the study area. For the low and high global warming scenarios, 50% (8 of 16) of the GCMs project an increase in total average annual precipitation for 2050 relative to 1990 at the western study area sites, while 63% (10 of 16) project an increase in total average annual precipitation at the eastern study area sites (App. 1). However, the median value of total average annual precipitation from all 16 GCMs shows statistical significance (p-value = 0.0160)(Table 4) between the west and east sites or between the low and high global warming scenarios (Fig. 2a) (Table 4). The western study area is projected to have <1% decrease in total average annual precipitation relative to historical values for both the low and high global warming scenarios (Fig. 2b). The eastern study area is projected to have a 3% and 1% increase in total average annual precipitation relative to historical values for the low and high warming scenarios, respectively (Fig. 2b).

Output from the GCMs overwhelming indicates greater annual irrigation for 2050 relative to 1990 across the study area. For the low global warming scenario, 81% (13 of 16) of the GCMs project an increase in annual irrigation at the WIC site, and 88% (14 of 16) project an increase at the EIC site (App. 2). For the high global warming scenario, 100% (16 of 16) of the GCMs project an increase in annual irrigation for the WIC and EIC sites (App. 2). Similar to historical irrigation patterns, the projected annual irrigation is significantly greater at the WIC than the EIC for the high (p-value < 0.001) and low warming (p-value < 0.001) scenarios (Fig. 3a) (Table 5). Under the high warming scenario, there is a projected median increase of nearly 15% and 14% relative to 1990 at the WIC and EIC sites, respectively, while under the low warming scenario, there is a projected median increase of approximately 2% and 1% relative to 1990 at the WIC and EIC sites (Fig. 3b).

Output from the GCMs indicates a substantial difference in projected annual ET depending on the warming scenario and LULC. For the low warming scenario, 56% (9 of 16) of the GCMs project an increase in average annual ET at the WR site (App. 3a), while only 6% (1 of 16) project an increase at the WIC site (App. 3b). For the low global warming scenario, 44% (7 of 16) of the GCMs project an increase in average annual ET at the ER site (App. 3a), and 94% (15 of 16) project an increase at the EIC site (App. 3b). For the high global warming scenario, 100% (16 of 16) of the 16 GCMs project an increase in average annual ET at all four sites (App. 3a,b). There are no statistical differences in median annual ET between the western (p-value = 0.412) and eastern (p-value = 0.877) study sites projected under the low global warming scenario (Fig. 4a,b) (Table 6). The median annual ET is projected to increase by 2% relative to 1990 values at the WR and WIC sites (Fig. 4c,d), and increase by <1% at the ER site and about 2% at the EIC site (Fig. 4c,d). However, there are statistical differences in median annual ET between the western (p-value = <0.001) and eastern (p-value = <0.001) sites projected under the high warming scenario (Fig. 4a,b) (Table 6). The median annual ET is projected to increase by about 21% and 7% relative to 1990 values at the WR and WIC sites, respectively (Fig. 4c,d), and increase by about 25% and 10% at the ER and EIC sites, respectively (Fig. 4c,d).

Output from the GCMs and HYDRUS-1D models overwhelming indicate decreases in annual recharge for 2050 relative to 1990 across the study area and beneath both types of LULC. For the low warming scenario, 56% (9 of 16) of the GCMs project a decrease in average annual recharge rates at the WR site (App. 4a), while 100% (16 of 16) project a decrease at the WIC site (App. 4b). For the low warming scenario, 44% (7 of 16) of the GCMs project a decrease in average annual recharge rates at the ER site (App. 4a), and 88% (14 of 16) project a decrease at the EIC site (App. 4b). For the high warming scenario, 94% (15 of 16) of the GCMs project a decrease in average annual recharge rates at the WR site (App. 4a), and 75% (12 of 16) project a decrease at the WIC site (App. 4b). For the high warming scenario, 94% (15 of 16) of the GCMs project a decrease in average annual recharge rates at the ER and EIC sites (App. 4a,b). There are no statistical differences in average annual recharge rates between the western (p-value = 0.0750) or eastern (p-value = 0.379) study sites projected under the low global warming scenario (Fig. 5a; 5b) (Table 7). The median annual recharge is projected to decrease by about 9% and 11% relative to 1990 values at the WR and WIC sites, respectively (Fig. 5c,d), and increase by 6% and decrease by 10% at the ER and EIC sites, respectively (Fig. 5c,d). However, there are statistical differences in median annual recharge rates between the western (p-value = <0.001) and eastern (p-value = <0.001) study sites projected under the high global warming scenario (Fig. 5a,b) (Table 7). The median annual recharge is projected to decrease by about 98% and 29% relative to 1990 values at the WR and WIC sites, respectively (Fig. 5c,d), and decrease by about 53% and 47% at the ER and EIC sites, respectively (Fig. 5c,d).

5.0 Discussion

The large range of projected precipitation (App. 1), irrigation (App. 2), and ET (App. 3) from the 16 GCMs indicates that using output from any single GCM or small group of GCMs to drive hydrologic models such as HYDRUS-1D would result in substantial uncertainty in the simulated recharge rates (App. 4) (Crosbie et al. 2011). This study minimizes uncertainty by using output from a large number of GCMs to estimate future recharge in a probabilistic framework (Crosbie et al. 2010). Additional uncertainty in the probabilistic framework has been reduced by calibrating the hydrologic model (HYDRUS-1D) with detailed hydraulic data from the vadose zone, and validating the hydrologic model with field-based recharge rates using a series of standard estimation methods. However, even with a well-calibrated hydrologic model, uncertainty in the output from 16 GCMs translates into a 5% to 70% range in projected recharge under any given LULC, east-west precipitation gradient, or warming scenario (Fig. 5c,d). In this study, recharge beneath the rangeland is projected to have the least (5%, WR site) and greatest (70%, ER site) range in projected recharge under the high warming scenario. The models tend to agree that the rangeland in the western study area will experience substantial decreases in recharge, while the models are less confident in the magnitude of the decrease in recharge beneath rangeland in the eastern study area.

The combined output from the probabilistic framework clearly indicates important differences in projected climate and recharge under the low (+1.0°C) and high (+2.4°C) warming scenarios. Under the low warming scenario, the distributions of annual precipitation, irrigation demands, ET, and recharge rates for a projected 2050 future, relative to historical 1990, are not statistically different. However, under the high warming scenario, the distributions of annual precipitation, irrigation demands, ET, and recharge rates for a projected 2050 future, relative to historical 1990, are statistically different. These findings indicate an important threshold or tipping point between +1.0°C and +2.4°C warming in the northern High Plains that could trigger significant changes in local hydrology and recharge.

As of May 2013, atmospheric CO_2 levels reached 400 ppm (National Oceanic and Atmospheric Administration 2013b), which represents a 12% increase since 1990 levels (354.35 ppm). From 1959 to 1990 (31 years), atmospheric CO_2 increased by 12%. Therefore, if current trends of increasing atmospheric CO_2 continue, 2050 levels will be greater than 650 ppm, which is a 15% increase over the high warming scenario (567 ppm) that was used in this study. A future warming scenario with 654 ppm CO_2 would likely result in even greater reduction of recharge rates to the northern High Plains.

Findings from this study are generally consistent with the (i) inverse relation between average annual air temperature and historical recharge rates along the regional north-south gradient of the entire High Plains aquifer (McMahon et al. 2006), and the (ii) positive relation between average annual precipitation and historical recharge along the west-east gradient of the northern High Plains (Steele et al. in review). However, this study demonstrates an important and substantial bidirectional (west to east and south to north) shift in median recharge rates of the northern High Plains aquifer in response to the high warming scenario. First, the projected 2050 air temperature for the northern High Plains is similar to that of present-day central High Plains (Fig. 1), which results in a substantial decrease in recharge rates at all study sites (Fig. 5c,d) that are similar to historical recharge rates for the central High Plains aquifer (McMahon et al. 2006). Second, the projected 2050 recharge rates for the eastern study area are lower than the historical recharge rates for the western study area (Fig. 5a,b), and the projected 2050 recharge rates for the western study area are similar to that of the southern and central High Plains (McMahon et al. 2006). Interestingly, the eastward shift in median recharge rate is less a function of projected changes in precipitation (Fig. 2) and more a function of the projected eastward shift in ET (Fig. 4a,b). Unlike temperature and ET, projected 2050 total annual precipitation is statistically the same as 1990 values for the eastern and western sites (Fig. 2a,b) (Table 4), which highlights the sensitivity of projected recharge to shifting ET regimes.

The probabilistic framework of simulated recharge rates has the additional benefits of helping to communicate findings to groundwater managers that are planning for sustainable development of local groundwater resources in the northern High Plains. For example, the distribution of future recharge rates (Fig. 5a-d) helps communicate the concept of uncertainty, and enables groundwater managers to select various percentiles

(5% and 95%; 10% and 90%, etc.) from the distributions as scenarios in groundwater models and other management planning tools. Regardless of the specific percentiles, groundwater managers in the northern High Plains must prepare for substantial reductions in future recharge rates beneath rangeland and irrigated corn fields. Higher temperatures and increased ET will alter the timing of demand for irrigation water, as different crops are grown in response to climate change (Karl et al. 2009). Local groundwater managers must continue working with growers to plant increasingly water-efficient and heat-tolerant crops that will directly reduce the irrigation demand. The reductions in recharge rates could accelerate declining water levels if irrigation demand and other management strategies aren't implemented. Because the bidirectional shift in climate and recharge is regional in nature, groundwater managers must continue to develop communication networks and educational opportunities to share and learn from best-management strategies and irrigation practices in neighboring groundwater management districts.

6.0 Conclusions

The first objective of this study was to use field-based recharge estimates to investigate recharge rates under different LULC and across an east-west precipitation gradient in the northern High Plains. The second objective was to use HYDRUS-1D and 16 different GCMs, each with two global warming scenarios, to simulate atmospheric and subsurface processes at the four northern High Plains study sites. The model outputs were used to produce a probabilistic framework of projections in precipitation, irrigation demands, ET and recharge rates under a 2050 climate relative to a 1990 climate. The third objective was to understand how climate change could shift regional climate along both east-west and north-south climate gradients.

The 16 GCMs, together with two global warming scenarios, were used to produce 32 projections of future precipitation, ET and recharge rates for each of the four study sites, and 32 projections of future irrigation demands at the two irrigated corn sites. The low-global-warming scenario showed no statistical evidence for a change in any future climate variable. However, the high-global-warming scenario showed significant changes, with statistically-significant evidence for decreases in average annual recharge rates, and increases in average annual ET and irrigation demands at all four study sites. Precipitation under the high-global-warming scenario did not show statistical evidence for a change from historical median annual values. Median annual irrigation demands increased by as much as 15%, median annual ET increased by as much as 25% and median annual recharge rates decreased as much as 98%, compared to simulated historical annual averages.

The major finding from this study is the projected bidirectional shift in climate and corresponding recharge rates in the northern High Plains. The north-south temperature gradient is projected to shift north, where future northern High Plains temperatures will resemble current central High Plains temperatures. The east-west recharge rate gradient is projected to shift east, where future recharge rates at the eastern study sites will resemble current recharge rates at the western study sites. Recharge rates under a future climate are particularly sensitive to ET. The east-west ET gradient will shift west, where future ET at the western study sites will resemble current ET at the eastern study sites. With higher ET and no change in precipitation, irrigation demands will increase, adding further stress on the groundwater resources in the northern High Plains.

7.0 References

Allison GB, Hughes MW (1978) The use of environmental chloride and tritium to estimate total recharge to an unconfined aquifer: Australian J of Soil Res 16(2): 181–195

Carrera-Hernández JJ, Smerdon BD, Mendoza CA (2012) Estimating ground water recharge through unsaturated flow modeling; sensitivity to boundary conditions and vertical discretization. J Hydrol 452–453: 90–101 pp. doi: 10.1016/j.jhydrol.2012.05.039

Chiew FHS, Teng J, Vaze J et al (2009) Estimating climate change impact on runoff across southeast Australia: method, results, and implications of the modeling method. Water Resour Res 45(W10414): 17 pp

Conservation Research Insititute (1995) Root systems of prairie plants. United States Department of Agriculture Natural Resources Conservation Service. Accessed April 17, 2013, from http://www.il.nrcs.usda.gov/technical/plants/npg/NPG-rootsystems.html

Crosbie RS, McCallum JL, Walker GR, Chiew FHS (2010) Modeling the climate change impact on groundwater recharge in the Murrey-Darling Basin. Hydrol J 18(7): 1639–1656. doi: 10.1007/s10040-010-0625-x

Crosbie RS, Dawes WR, Charles SP et al (2011) Differences in future recharge estimates due to GCMs, downscaling methods and hydrological models. Geophys Res Lett 38(11): L11406. doi: 10.1029/2011GL047657

Crosbie RS, Scanlon BR, Mpelasoka FS et al (2013) Potential climate change impacts on groundwater recharge in the high plains aquifer, USA. Water Resour Res. doi: 10.1002/wrcr.20292

Delin GN, Healy RW, Landon MK, Böhlke JK (2000) Effects of topography and soil properties on recharge at two sites in an agricultural field: J Amer Water Res Assoc 36(6): 1401–1416

Delin GN, Healy RW, Lorenz DL, Nimmo JR (2007) Comparison of local- to regional-scale estimates of ground-water recharge in Minnesota, USA: J Hydrol 334(1–2): 231–249

Dennehy KF, Litke DW, McMahon PB (2002) The High Plains aquifer, USA: Groundwater development and sustainability. P.99-119. In Hiscock KM, Rivett MO, Davidson RM (ed.) Sustainable groundwater development. Geol Soc of London Special Pub 193. Geol Soc Pub House, London, UK

Dettinger MD, Earman S (2007) Western ground water and climate change - pivotal to supply sustainability or vulnerable in its own right? Ground Water News Views 4: 4–5

Döll P, Fiedler K (2008) Global-scale modeling of groundwater recharge. Hydrol Earth Syst Sci 12: 863–885

Döll P (2009) Vulnerability to the impact of climate change on renewable groundwater resources: a global-scale assessment. Environ Res Lett 4: 035006. doi: 10.1088/1748-9326/4/3/035006

Earman S, Dettinger M (2011) Potential impacts of climate change on groundwater resources – a global review. J of Water and Clim Change 2: 213. doi: 10.2166/wcc.2011.034

Food and Agriculture Organization of the United Nations (1998) Crop evapotranspiration – Guidelines for computing crop water requirements. Document prepared by Allen RG, Pereira LS, Raes D et al. Accessed April 17, 2013, from http://www.fao.org/docrep/X0490E/x0490e00.htm#Contents

Feddes RA, Kowalik PJ, Zaradny H (1978), Simulation of Field Water Use and Crop Yield, John Wiley & Sons, New York, NY

Flint AL, Campbell GS, Ellett KM et al (2002) Calibration and temperature correction of heat dissipation matric potential sensors. Soil Sci Soc Am J 66: 1436–1445

Green TR, Taniguchi M, Kooi H et al (2011) Beneath the surface of global change: Impacts of climate change on groundwater. J of Hydrol 405:532–560. doi: 10.1016/j.jhydrol.2011.05.002

Gurdak JJ, Hanson RT, McMahon PB et al (2007) Climate Variability Controls on Unsaturated Water and Chemical Movement, High Plains Aquifer, USA. Vadose Zone J 6(3): 533. doi:10.2136/vzj2006.0087

Gurdak JJ, Walvoord MA, McMahon PB (2008) Susceptibility to enhanced chemical migration from depression-focused preferential flow, High Plains Aquifer. Vadose Zone J 7(4): 1172–1184

Gurdak JJ, McMahon PB, Dennehy KF et al (2009) Water quality in the High Plains Aquifer, Colorado, Kansas, Nebraska, New Mexico, Oklahoma, South Dakota, Texas, and Wyoming, 1999–2004: USGS Circ 1337: 63 p

Gurdak JJ, McMahon PB, Bruce BW (2012) Vulnerability of groundwater quality to human activity and climate change and variability, High Plains aquifer, USA, In Treidel H, Martin-Bordes JJ, Gurdak JJ(Eds.). Climate change effects on groundwater resources: A global synthesis of findings and recommendations, IAH - International Contributions to Hydrogeology, Taylor and Francis publishing, 414 p., ISBN 978-0415689366

Gutentag ED, Heimes FJ, Krothe NC et al (1984) Regional aquifer-system analysis of the High Plains aquifer in parts of Colorado, Kansas, Nebraska, New Mexico, Oklahoma, South Dakota, Texas, and Wyoming. Geohydrology, USGS Prof Pap 1400–B, 63 pp

Hanson RT, Flint LE, Flint AL et al (2012) A method for physically based model analysis of conjunctive use in response to potential climate changes. Water Resour Res doi: 10.1029/2011WR010774

Healy RW (2010) Estimating Groundwater Recharge, Cambridge Univ Press, Cambridge, United Kingdom, 245 p

Hendriks MR (2010) Introduction to physical hydrology, Oxford Univ Press Inc, New York, NY, 331 p

Herbel MJ, Spalding RF (1993) Vadose zone fertilizer derived nitrate and δ15N extracts: Ground Water 31: 376–382

Holman I, Allen D, Cutthbert M et al (2012) Towards best practice for assessing the impacts os climate change on groundwater. Hydrogeol J 20(1):1–4. doi: 10.1007/s10040-011-0805-3

IPCC (2007) Climate Change 2007: The Physical Science Basis. Contribution of Working Group 1 to the Fourth Assessment Report of the Intergovernmental Panel on Climate Change. 996 pp. Cambridge Univ Press, Cambridge UK

Kalnay E, Kanamitsu M, Kistler R et al (1996) The NCEP/NCAR 40-year reanalysis project. Bulletin of the Am Meteo Soc 77(3): 437-471

Karl TR, Melillo JM, Peterson TC (2009) Global Climate Change Impacts in the United States, 196 pp., Cambridge Univ Press, New York

Kromm DE, White SE (1992) The High Plains, Ogallala region. Univ Press of Kansas. pp. 1–27

Lindau CW, Spalding RF (1984) Major procedural discrepancies in soil extracted nitrate levels and nitrogen isotopic values: Ground Water 22: 273–278

Luckey RR, Cannia JC (2006) Groundwater flow model of the Western Model Unit of the Nebraska Cooperative Study (COHYST) Area: Cooperative Hydrology Study Technical Committee, 63 p

Maurer EP, Wood AW, Adam JC et al (2002) A Long-Term Hydrologically-Based Data Set of Land Surface Fluxes and States for the Conterminous United States, J Clim 15: 3237-3251

Maupin MA, Barber NL (2005) Estimated withdrawals from principal aquifers in the United States, 2000. Circ 1279. USGS, Reston, VA

McGuire VL, Johnson MR, Schieffer RL et al (2003) Water in storage and approaches to ground-water management, High Plains aquifer, 2000. Circ 1243. USGS, Reston, VA

McMahon PB, Dennehy KF, Michel RL et al (2003) Water movement through thick unsaturated zones overlying the central High Plains aquifer, southwestern Kansas, 2000–2001. Available at pubs.usgs.gov/wri/wrir03-4171/ (verified 12 Aug. 2008). Water-Resour Invest Rep 03-4171. USGS, Reston, VA

McMahon PB, Dennehy KF, Bruce BW et al (2006) Storage and transit time of chemicals in thick unsaturated zones under rangeland and irrigated cropland, High Plains, United States. Water Resour Res 42(3): n/a–n/a. doi:10.1029/2005WR004417

McMahon PB, Dennehy KF, Bruce BW et al (2007) Water-quality assessment of the High Plains aquifer, 1999-2004, USGS Professional Paper 1749, 212 pp

Meehl GA, Covey C, Delworth T et al (2007) The WCRP CMIP3 multimodel dataset: a new era in climate change research. Bull Am Meteorol Soc 88(9):1383–1394

Monteith JL (1981) Evaporation and surface temperature, Quarterly J Royal Meteo Soc 107: 1-27

Monteith JL, Unsworth MH (1990) Principles of Environmental Physics, Edward Arnold, London

Nakicenovic N, Swart N (2000) Special Report on Emission Scenarios, 612 pp, Intergovernmental Panel on Climate Change

National Oceanic and Atmospheric Administration (2013a) National Climatic Data Center, annual data, United States, January 2013: National Oceanic and Atmospheric Administration, information available on Web, accessed January 2013, at http://www.ncdc.noaa.gov/cdo-web/#t=secondTabLink

National Oceanic and Atmospheric Administration (2013b) National Climatic Data Center, State of the Climate: Global Analysis for March 2013, published online April 2013, retrieved on March 18, 2013 from http://www.ncdc.noaa.gov/sotc/global/

Nebraska Department of Natural Resources (2010) 2011 Annual evaluation of availability of hydrologically connected water supplies. Document prepared by J. Bradley, B. Flyr, J. Gilbert, P. Goltl, D. Hallum, A. Kessler, P. Koester, J. Lear, L. Paeglis, M. Pun, J. Schellpeper, K. Schwartman, R. Vollertsen, A. Wright, T. Zayac, and S Zheng. Accessed April 18, 2013, from http://dnr.ne.gov/IWM/AnnualReport/AnnualReport_2011.html

Neuman SP, Feddes RA, Bresler E (1974) Finite element simulation of flow in saturatedunsaturated soils considering water uptake by plants, Third Annual Report, Project No. A10-SWC-77, Hydraulic Engineering Lab., Technion, Haifa, Israel, 1974

Phillips F (1994) Environmental tracers for water movement in desert soils of the American Southwest. Soil Sci Soc of Am J 58:15–24

Qi SL, Konduris A, Litke DW et al (2002) Classification of irrigated land using satellite imagery, the High Plains aquifer, nominal date 1992. Available at pubs.usgs.gov/wri/wrir02-4236/ (verified 12 Aug. 2008). 1183 Water-Resour Invest Rep 02-4236. USGS, Reston, VA

Richards L (1931) Capillary conduction of liquids in porous mediums. Physics 1: 318–333

Sandstrom K (1995) Modeling the effects of rainfall variability on groundwater recharge in semi-arid Tanzania. Nordic Hydrol 26:313–330

Scanlon BR, Healy RW, Cook PG (2002) Choosing appropriate techniques for quantifying groundwater recharge. Hydrogeol J 10(1):18–39

Scanlon BR, Reedy RC, Stonestrom DA et al (2005) Impacts of land use and land cover change on groundwater recharge and quality in the southwestern USA. Global Change Biol 11:1577–1593. doi:10.1111/j.1365-2486.2005.01026.x

Scanlon BR, Keese KE, Flint AL et al (2006) Global synthesis of groundwater recharge in semiarid and arid regions. Hydrol Process 20:3335–3370. doi: 10.1002/hyp.6335

Scanlon BR, Faunt CC, Longuevergne L et al (2012) Groundwater depletion and sustainability of irrigation in the US High Plains and Central Valley. P Natl A Sci 109(24): 9320–9325. doi: 10.1073/pnas.1200311109

Schaap MG, Leij FJ, van Genuchten MTh (2001) Rosetta: a computer program for estimating soil hydraulic parameters with hierarchical pedotransfer functions. J of Hydrol 251:163-176

Ŝimůnek J, van Genuchten MTh, Sejna M (2008) Development and applications of the X beneath native vegetation, irrigated fields, and the Amargosa River channel, Amargosa Desert, Nye County, Nevada, USGS Open File Rep, 03–104, 82 pp

Small EE (2005) Climatic controls on diffuse groundwater recharge in semiarid environments of the southwestern United States. Water Resour Res 41:W04012. doi: 10.1029/2004WR003193

Soil Survey Staff (1999) Soil taxonomy—a basic system of soil classification for making and interpreting soil surveys (2d ed.): Natural Resources Conservation Service, US Department of Agriculture Handbook 436, 871 p., also available at http://soils.usda.gov/technical/classification/taxonomy

Sophocleous M (2012) Conserving and extending the useful life of the largest aquifer in North America; the future of the High Plains/Ogallala Aquifer. Ground Water 50(6):831–839. doi: 10.1111/j.1745-6584.2012.00965.x

Steele GV, Gurdak JJ, Hobza CM (in review) Water movement through the unsaturated zone of the High Plains aquifer in the Central Platte Natural Resources District, Nebraska, 2008–12. USGS Scientific Report Series 201X–52XX

Szilagyi J, Zlotnik VA, Gates JB, Jozsa J (2001) Mapping mean annual groundwater recharge in the Nebraska Sand Hills, USA, Hydrogeol J 19(8): 1503–1513. doi: 10.1007/s10040-011-0769-3

Taylor RG, Scanlon BR, Döll P et al (2012) Ground water and climate change. Nat Clim Change 3:322–329. doi: 10.1038/nclimate1744

Thatcher LL, Janzer VJ, Edwards KW (1977) Methods for determination of radioactive substances in water and fluvial sediment, USGSTech Water Resour Invest, Book 5, Chap. A5, 95 pp

University of Nebraska-Lincoln (2010) Native vegetation of Nebraska. University of Nebraska State Museum. Retrieved April 17, 2013, from http://museum.unl.edu/research/botany/nebraska_vegetation.html

van Genuchten MTh (1980) A closed form equation for predicting the hydraulic conductivity of unsaturated soils, Soil Sci Soc Am J 44: 892–898

Wada Y, van Beek LPH, van Kempen CM et al (2010) Global depletion of groundwater resources. Geophys Res Lett 37:n/a–n/a. doi: 10.1029/2010GL044571

Wanielista M, Kersten R, Eaglin R (1997) Hydrology Water Quantity and Quality Control. John Wiley & Sons. 2nd ed

Wesseling JG, Elbers JA, Kabat P, van den Broek BJ (1991) SWATRE: instructions for input, Internal Note, Winand Staring Centre, Wageningen, the Netherlands, 1991

Woldeamlak ST, Batelaan O, De Smedt F (2007) Effects of climate change on the groundwater system in the Grote-Nete catchment, Belgium. Hydrogeol J 15:891–901. doi: 10.1007/s10040-006-0145-x

TABLES

Table 1: Vadose zone monitoring sites in the Central Platte Natural Resources District Unsaturated-Zone Network (2008-2013) used in this study [bls, below land surface; m, meters; altitude above the North American Vertical Datum of 1988; latitude and longitude North American Datum of 1983].

Site	USGS Site ID	Water level bls (m)	Altitude (m)	Latitude	Longitude
eastern rangeland (ER)	410102098374201	20	606.6	41°01'02.5"	-98°37'41.7"
eastern irrigated corn (EIC)	405855098383001	30	618.1	40°58'55.4"	-98°38'30.1"
western rangeland (WR)	405738099504501	15	777.8	40°57'38.3"	-99°50'44.8"
western irrigated corn (WIC)	405855100073901	18	803.1	40°58'54.7"	100°07'38.8"

Table 2: List of 16 global climate models (GCMs) used in this study and abbreviations used in Figures [CMIP3 I.D., Coupled Model Intercomparison Project phase 3 model identification] (Modified from Crosbie et al. 2013).

Organization	**Country**	**CMIP3 I.D.**	**Abbreviation**
Bjerknes Centre for Climate Research	Norway	BCCR-BCM2.0	BCCR
Canadian Centre for Climate Modelling & Analysis	Canada	CGCM3.1(T63)	CCCMA
Météo-France / Centre National de Recherches Météorologiques	France	CNRM-CM3	CNRM
CSIRO Atmospheric Research	Australia	CSIRO-Mk3.0	CSIRO MK3.0
CSIRO Atmospheric Research	Australia	CSIRO-Mk3.5	CSIRO MK3.5
US Dept. of Commerce / NOAA / Geophysical Fluid Dynamics Laboratory	USA	GFDL-CM2.0	GFDL CM2.0
US Dept. of Commerce / NOAA / Geophysical Fluid Dynamics Laboratory	USA	GFDL-CM2.1	GFDL CM2.1
NASA / Goddard Institute for Space Studies	USA	GISS-ER	GISS
Instituto Nazionale di Geofisica e Vulcanologia	Italy	INGV-SXG	INGV
Institute for Numerical Mathematics	Russia	INM-CM3.0	INMCM
Institut Pierre Simon Laplace	France	IPSL-CM4	IPSL
Center for Climate System Research (The University of Tokyo), National Institute for Environmental Studies, and Frontier Research Center for Global Change (JAMSTEC)	Japan	MIROC3.2(medres)	MIROC
Max Planck Institute for Meteorology	Germany	ECHAM5/MPI-OM	MPI
Meteorological Institute of the University of Bonn, Meteorological Research Institute of KMA, and Model and Data group.	Germany / Korea	ECHO-G	MIUB
Meteorological Research Institute	Japan	MRI-CGCM2.3.2	MRI
National Center for Atmospheric Research	USA	PCM	NCAR

Table 3: Estimated diffuse recharge rates (mm yr^{-1}) from field-based tritium (^3H), chloride mass-balance, and potassium bromide tracer methods (modified from Steele et al. in review), and simulated conservative solute flux from the HYDRUS-1D models [–, estimates of diffuse recharge are not available because of either flushing of postbomb ^3H, uncertainties associated with chloride concentrations in applied irrigation water, or the apparent groundwater age predates age-dating methods (Steele et al. in review)].

Recharge methods	**western rangeland (WR)**	**eastern rangeland (ER)**	**western irrigated corn (WIC)**	**eastern irrigated corn (EIC)**
Tritium (^3H)				
center of mass (mm yr^{-1})	4	–	–	80
peak displacement (mm yr^{-1})	44	–	–	59
Chloride-mass balance (CMB)				
mean (mm yr^{-1})	13	21	–	–
range (mm yr^{-1})	1.1–68	1.8–96	–	–
Potassium bromide (KBr) tracer				
center of mass (mm yr^{-1})	35	38	65	207
peak displacement (mm yr^{-1})	201	9	65	172
mean of KBr methods (mm yr^{-1})	118	24	65	190
Groundwater-dating				
mean (mm yr^{-1})	34	24	224	–
HYDRUS-1D simulated tracer				
center of mass (range) (mm yr^{-1})	74–153	89–106	79–129	178–218
peak displacement (range) (mm yr^{-1})	100–166	37–109	78–128	180–215

Table 4: Wilcoxon signed-rank test for precipitation data to determine the median difference between paired observations equals zero. The table lists p-values for each paired comparison. Where the p-value is less than alpha-value of 0.05 (95% confidence level), the median values are statistically different [W, E, L, and H denote western study area, eastern study area, low-global-warming scenario, and high-global-warming scenario, respectively].

Figure 2a		W-1990	E-1990	W-L-2050	E-L-2050	W-H-2050
	E-1990	0.0160	--	--	--	--
	W-L-2050	0.830	0.0250	--	--	--
	E-L-2050	0.00500	0.610	0.00600	--	--
	W-H-2050	0.739	0.0320	0.773	0.0100	--
	E-H-2050	0.00100	0.340	0.00200	0.511	0.00200
Figure 2b				W-L-2050	E-L-2050	W-H-2050
			E-L-2050	<0.001	--	--
			W-H-2050	0.0240	<0.001	--
			E-H-2050	<0.001	<0.001	<0.001

Table 5: Wilcoxon signed-rank test for irrigation data to determine the median difference between paired observations equals zero. The table lists p-values for each paired comparison. Where the p-value is less than alpha-value of 0.05 (95% confidence level), the median values are statistically different [W, E, L, and H denote western study area, eastern study area, low-global-warming scenario, and high-global-warming scenario, respectively].

Figure 3a		W-1990	E-1990	W-L-2050	E-L-2050	W-H-2050
	E-1990	<0.001	--	--	--	--
	W-L-2050	0.404	<0.001	--	--	--
	E-L-2050	<0.001	0.706	<0.001	--	--
	W-H-2050	<0.001	<0.001	<0.001	<0.001	--
	E-H-2050	<0.001	<0.001	<0.001	<0.001	<0.001
Figure 3b				W-L-2050	E-L-2050	W-H-2050
			E-L-2050	<0.001	--	--
			W-H-2050	<0.001	<0.001	--
			E-H-2050	<0.001	<0.001	<0.001

Table 6: Wilcoxon signed-rank test for evapotranspiration data to determine the median difference between paired observations equals zero. The table lists p-values for each paired comparison. Where the p-value is less than alpha-value of 0.05 (95% confidence level), the median values are statistically different [W, E, L, H, and I denote western study area, eastern study area, low-global-warming scenario, high-global-warming scenario, and irrigated land, respectively].

Figure 4a&b	W-1990	E-1990	W-L-2050	E-L-2050	W-H-2050	E-H-2050	WIC-1990	EIC-1990	WIC-L-2050	EIC-L-2050	WIC-H-2050
E-1990	<0.001	--	--	--	--	--	--	--	--	--	--
W-L-2050	0.412	<0.001	--	--	--	--	--	--	--	--	--
E-L-2050	<0.001	0.877	<0.001	--	--	--	--	--	--	--	--
W-H-2050	<0.001	<0.001	<0.001	<0.001	--	--	--	--	--	--	--
E-H-2050	<0.001	<0.001	<0.001	<0.001	0.004	--	--	--	--	--	--
WIC-1990	<0.001	<0.001	<0.001	<0.001	<0.001	<0.001	--	--	--	--	--
EIC-1990	<0.001	<0.001	<0.001	<0.001	<0.001	<0.001	0.277	--	--	--	--
WIC-L-2050	<0.001	<0.001	<0.001	<0.001	<0.001	<0.001	0.264	0.066	--	--	--
EIC-L-2050	<0.001	<0.001	<0.001	<0.001	<0.001	<0.001	0.923	0.264	0.371	--	--
WIC-H-2050	<0.001	<0.001	<0.001	<0.001	<0.001	<0.001	<0.001	<0.001	<0.001	<0.001	--
EIC_H_2050	<0.001	<0.001	<0.001	<0.001	<0.001	<0.001	<0.001	<0.001	<0.001	<0.001	0.959
Figure 4c&d			W-L-2050	E-L-2050	W-H-2050	E-H-2050	--	--	WIC-L-2050	EIC-L-2050	WIC-H-2050
		E-L-2050	<0.001	--	--	--	--	--	--	--	--
		W-H-2050	<0.001	<0.001	--	--	--	--	--	--	--
		E-H-2050	<0.001	<0.001	<0.001	--	--	--	--	--	--
		WIC-L-2050	0.002	<0.001	<0.001	<0.001	--	--	--	--	--
		EIC-L-2050	<0.001	<0.001	<0.001	<0.001	--	--	0.0850	--	--
		WIC-H-2050	<0.001	<0.001	<0.001	<0.001	--	--	<0.001	<0.001	--
		EIC_H_2050	<0.001	<0.001	<0.001	<0.001	--	--	<0.001	<0.001	<0.001

Table 7: Wilcoxon signed-rank test for recharge data to determine the median difference between paired observations equals zero. The table lists p-values for each paired comparison. Where the p-value is less than alpha-value of 0.05 (95% confidence level), the median values are statistically different [W, E, L, H, and I denote western study area, eastern study area, low-global-warming scenario, high-global-warming scenario, and irrigated land, respectively].

Figure 5a&b	W-1990	E-1990	W-L-2050	E-L-2050	W-H-2050	E-H-2050	WIC-1990	EIC-1990	WIC-L-2050	EIC-L-2050	WIC-H-2050
E-1990	<0.001	--	--	--	--	--	--	--	--	--	--
W-L-2050	0.0750	<0.001	--	--	--	--	--	--	--	--	--
E-L-2050	<0.001	0.379	<0.001	--	--	--	--	--	--	--	--
W-H-2050	<0.001	<0.001	<0.001	<0.001	--	--	--	--	--	--	--
E-H-2050	<0.001	<0.001	0.0170	<0.001	<0.001	--	--	--	--	--	--
WIC-1990	<0.001	<0.001	<0.001	<0.001	<0.001	<0.001	--	--	--	--	--
EIC-1990	<0.001	<0.001	<0.001	<0.001	<0.001	<0.001	0.00400	--	--	--	--
WIC-L-2050	<0.001	<0.001	<0.001	<0.001	<0.001	<0.001	0.172	<0.001	--	--	--
EIC-L-2050	<0.001	<0.001	<0.001	<0.001	<0.001	<0.001	0.0590	0.240	0.0020	--	--
WIC-H-2050	<0.001	<0.001	<0.001	<0.001	<0.001	<0.001	0.001	<0.001	0.0240	<0.001	--
EIC_H_2050	<0.001	<0.001	<0.001	<0.001	<0.001	<0.001	<0.001	<0.001	0.0210	<0.001	0.900
Figure 5c&d			W-L-2050	E-L-2050	W-H-2050	E-H-2050	--	--	WIC-L-2050	EIC-L-2050	WIC-H-2050
		E-L-2050	<0.001	--	--	--	--	--	--	--	--
		W-H-2050	<0.001	<0.001	--	--	--	--	--	--	--
		E-H-2050	<0.001	<0.001	<0.001	--	--	--	--	--	--
		WIC-L-2050	0.228	<0.001	<0.001	<0.001	--	--	--	--	--
		EIC-L-2050	0.246	<0.001	<0.001	<0.001	--	--	0.00800	--	--
		WIC-H-2050	<0.001	<0.001	<0.001	<0.001	--	--	<0.001	<0.001	--
		EIC_H_2050	<0.001	<0.001	<0.001	0.356	--	--	<0.001	<0.001	<0.001

FIGURES

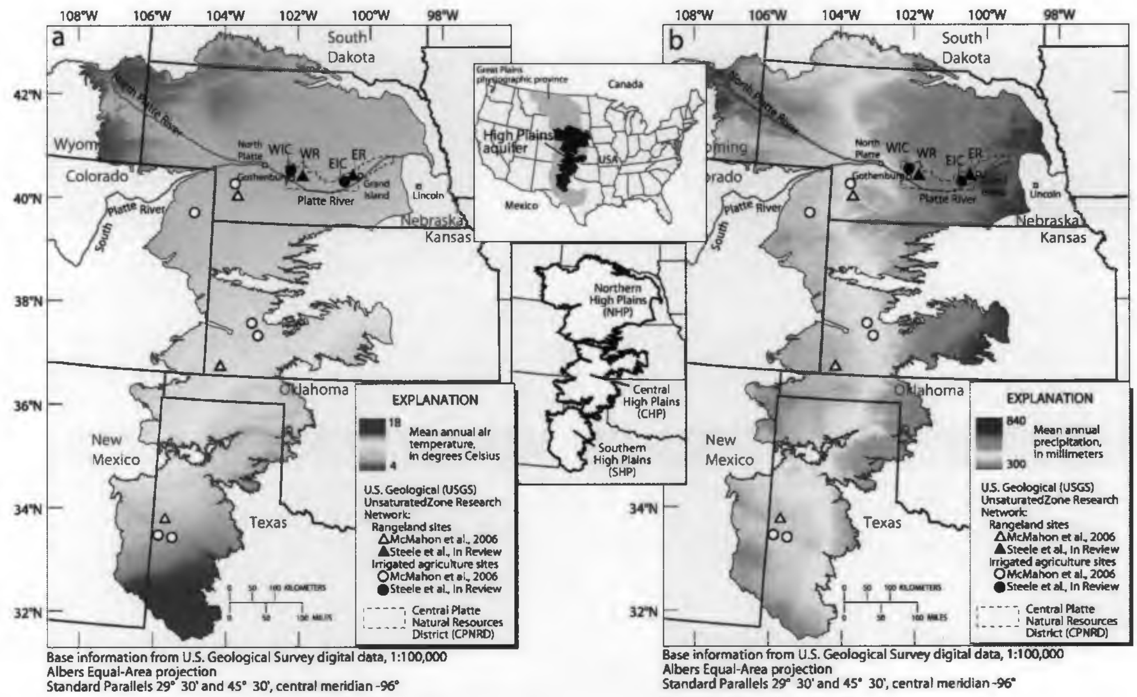

Figure 1: Location of the northern High Plains rangeland and irrigated agricultural study sites on the distribution of regional (a) mean annual air temperature and (b) mean annual precipitation (modified from McMahon et al., 2009). The study includes the eastern rangeland (ER), western rangeland (WR), eastern irrigated corn (EIC), and western irrigated corn (WIC) sites in the Central Platte Natural Resources District (CPNRD).

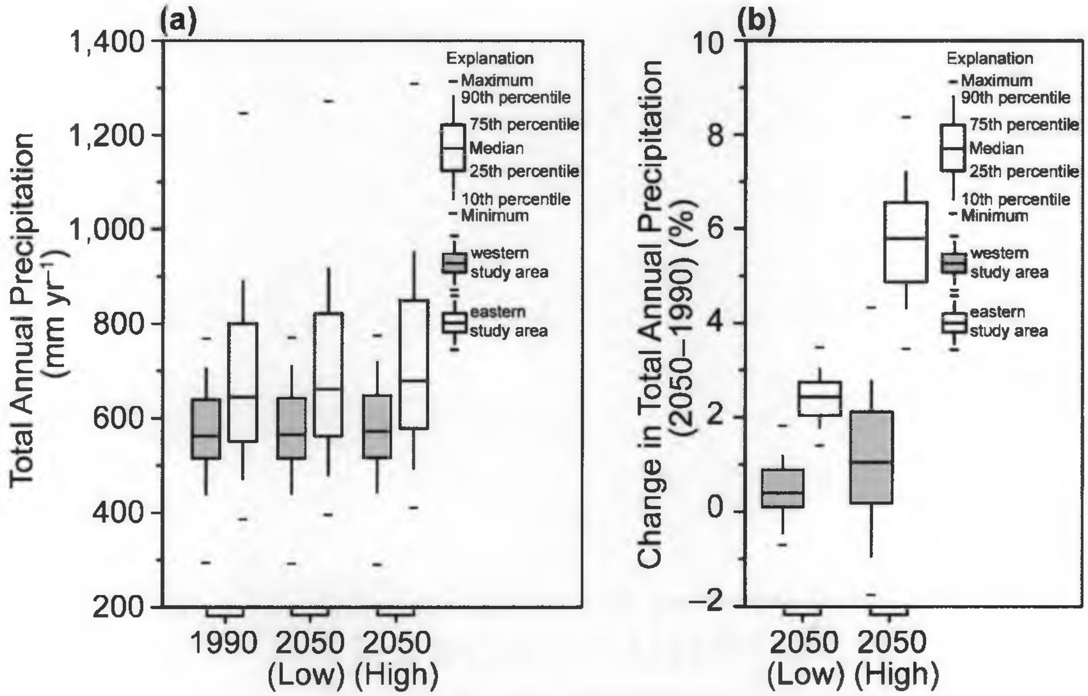

Figure 2: Observed historical (1990) and simulated future (2050) (a) total annual precipitation (mm yr^{-1}) and (b) percent (%) change in total annual precipitation at Gothenburg, Nebraska (western study area) and Grand Island, Nebraska (eastern study area) for low (+1.0°C, 478 ppm CO2) and high (+2.4°C, 567 ppm CO2) global warming scenarios. Each boxplot represents the median of 30 years of simulated precipitation from 16 global climate models (GCMs).

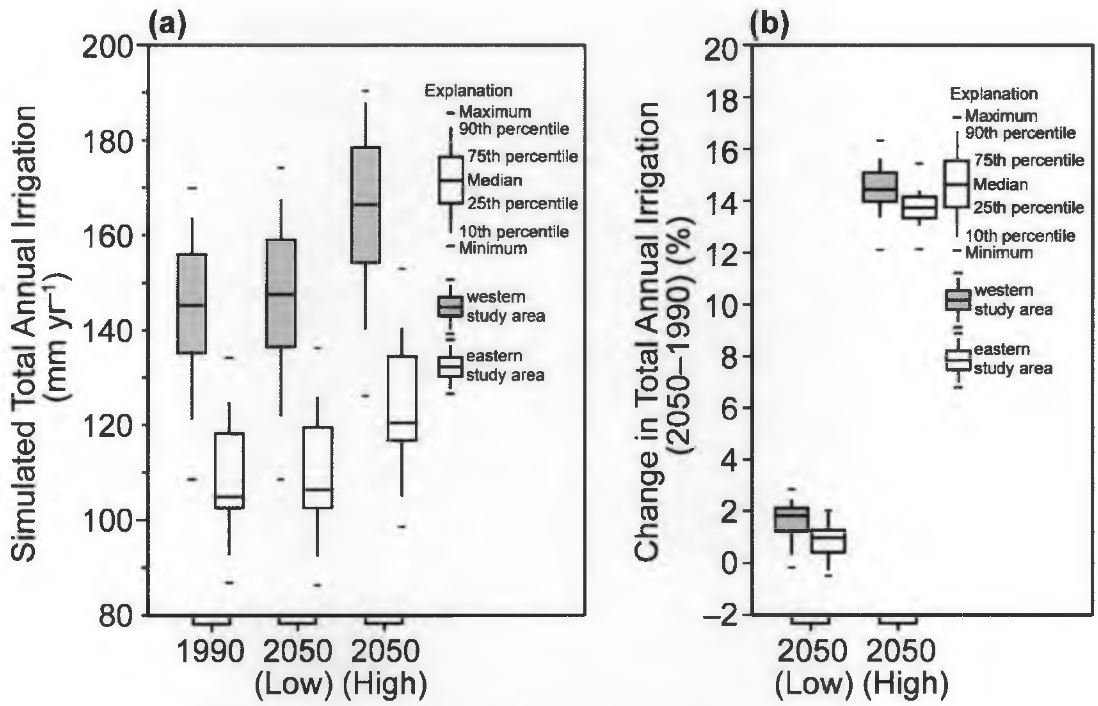

Figure 3: Simulated historical (1990) and future (2050) (a) total annual irrigation (mm yr–1) and (b) percent (%) change in total annual irrigation applied at the western (WIC) and eastern irrigated corn (EIC) sites for low (+1.0°C, 478 ppm CO2) and high (+2.4°C, 567 ppm CO2) global warming scenarios. Each boxplot represents the median of 30 years of simulated irrigation based on simulated average annual precipitation and air temperature from 16 global climate models (GCMs).

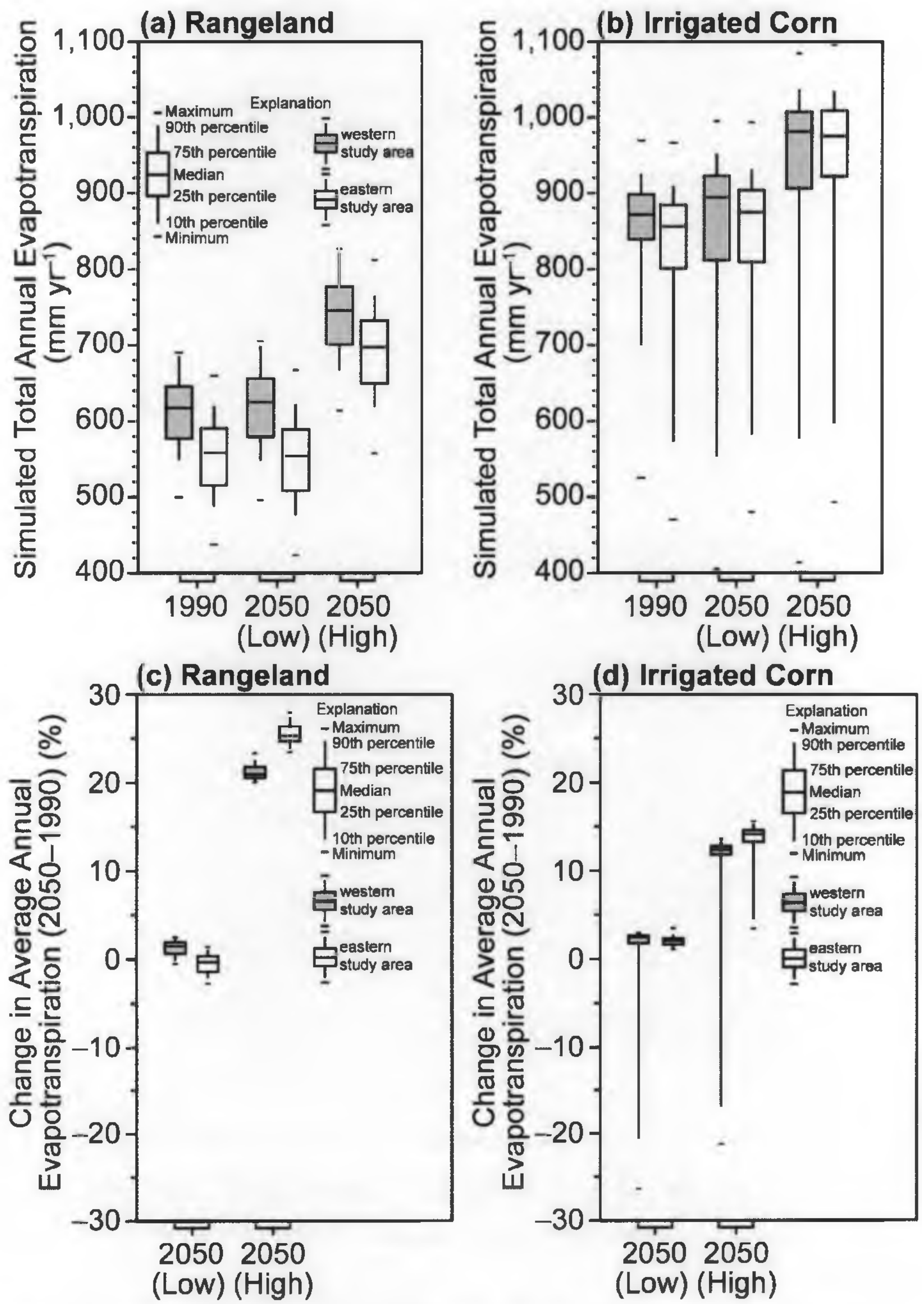

Figure 4: Simulated historical (1990) and future (2050) (a,c) total annual evapotranspiration (mm yr–1) and (b,d) percent (%) change in total annual evapotranspiration at the western and eastern study area sites beneath (a, c) rangeland and (b, d) irrigated corn for low (+1.0°C, 478 ppm CO_2) and high (+2.4°C, 567 ppm CO_2) global warming scenarios. Each boxplot represents the median of 30 years of simulated average annual evapotranspiration from 16 global climate models (GCMs).

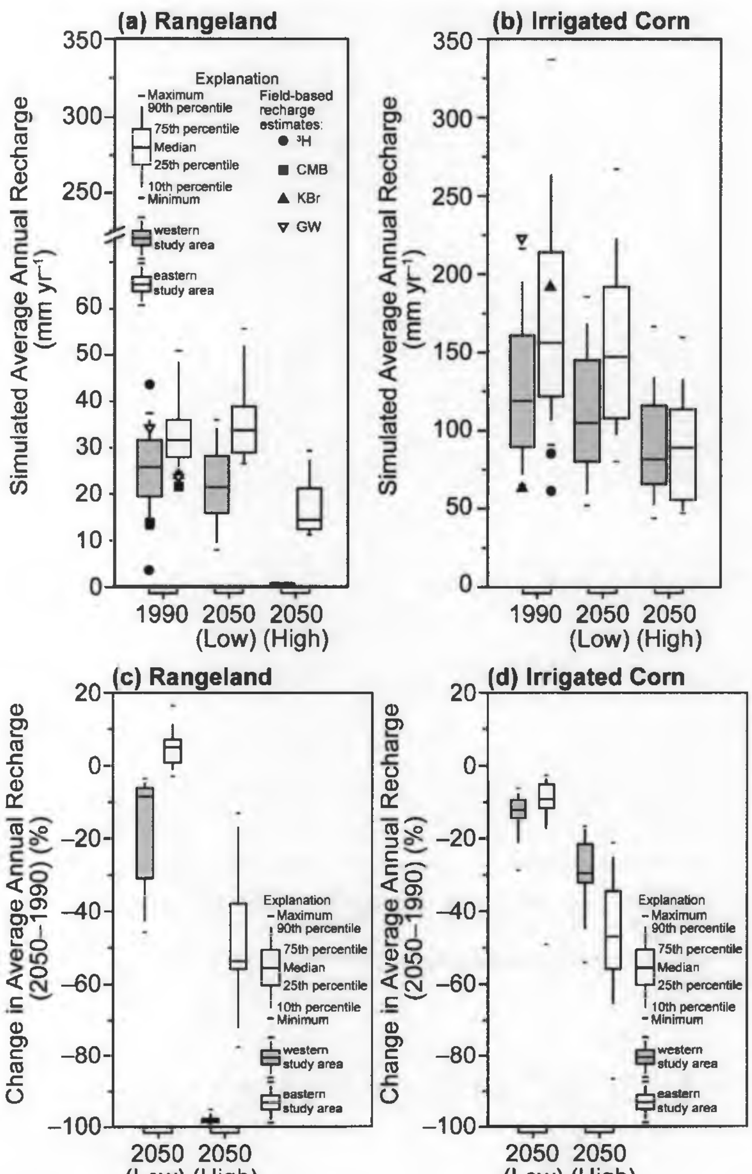

Figure 5: Simulated historical (1990) and future (2050) (a,c) average annual recharge (mm yr–1) and (b,d) percent (%) change in average annual recharge at the western and eastern study area sites beneath (a, c) rangeland and (b, d) irrigated corn for low (+1.0°C, 478 ppm CO2) and high (+2.4°C, 567 ppm CO2) global warming scenarios. Each boxplot represents the median of 30 years of simulated average annual recharge from 16 global climate models (GCMs). The field-based recharge estimates from tritum (^{3}H), chloride-mass balance (CMB), applied potassium bromide trace (KBr), and groundwater-age dating (GW) methods are listed in Table 3.

APPENDICES

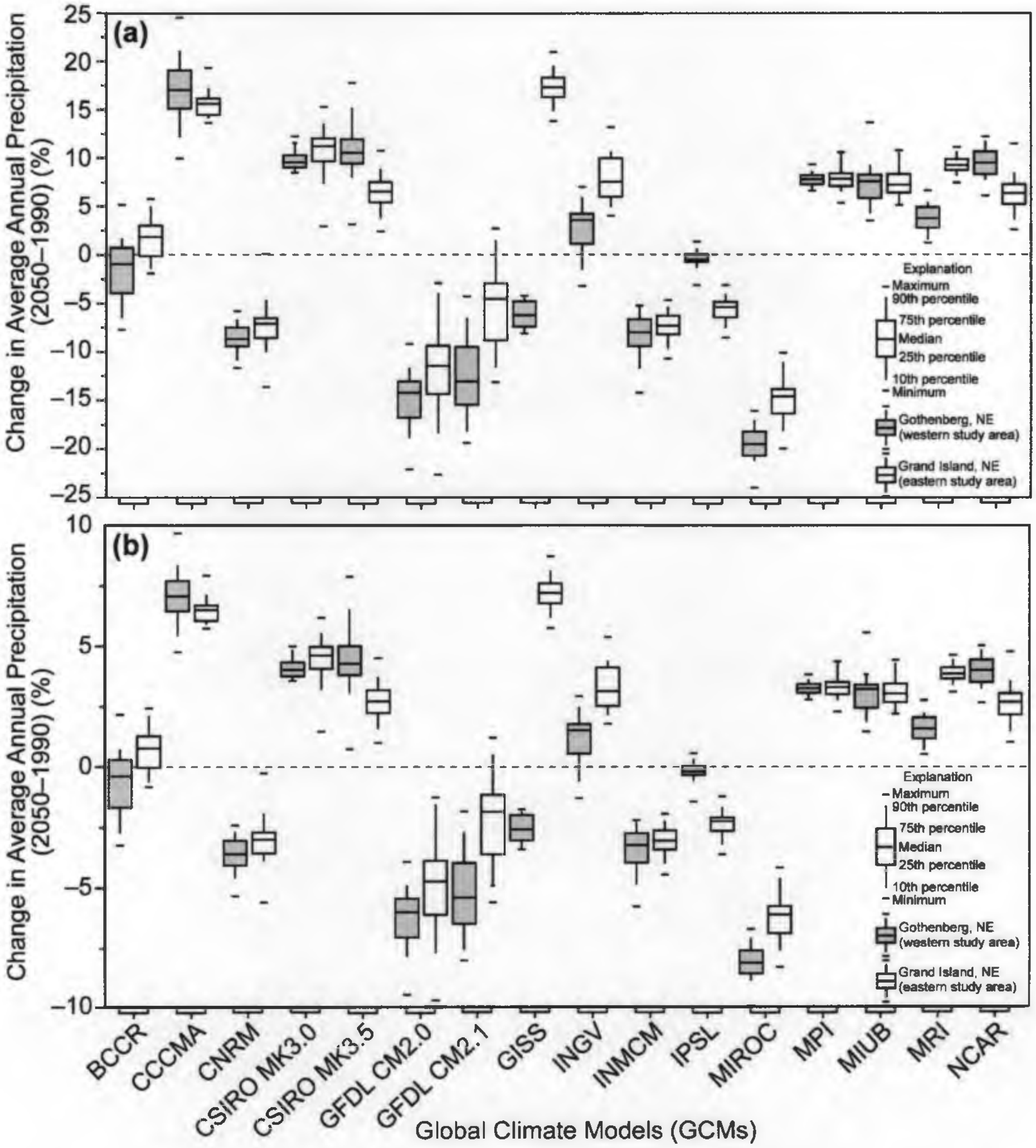

Appendix 1: Boxplots of the percent (%) change in simulated average annual precipitation between 2050 and 1990 at Gothenburg, Nebraska (western study area) and Grand Island, Nebraska (eastern study area) for (a) high global warming scenario (+2.4°C, 567 ppm CO2) and (b) low global warming scenario (+1.0°C, 478 ppm CO2) from 16 global climate models (GCMs). Each boxplot represents 30 years of simulated precipitation. The dashed line represents no change; positive values indicate greater future average annual precipitation and negative values indicate smaller future average annual precipitation. Note the different y-axis scales.

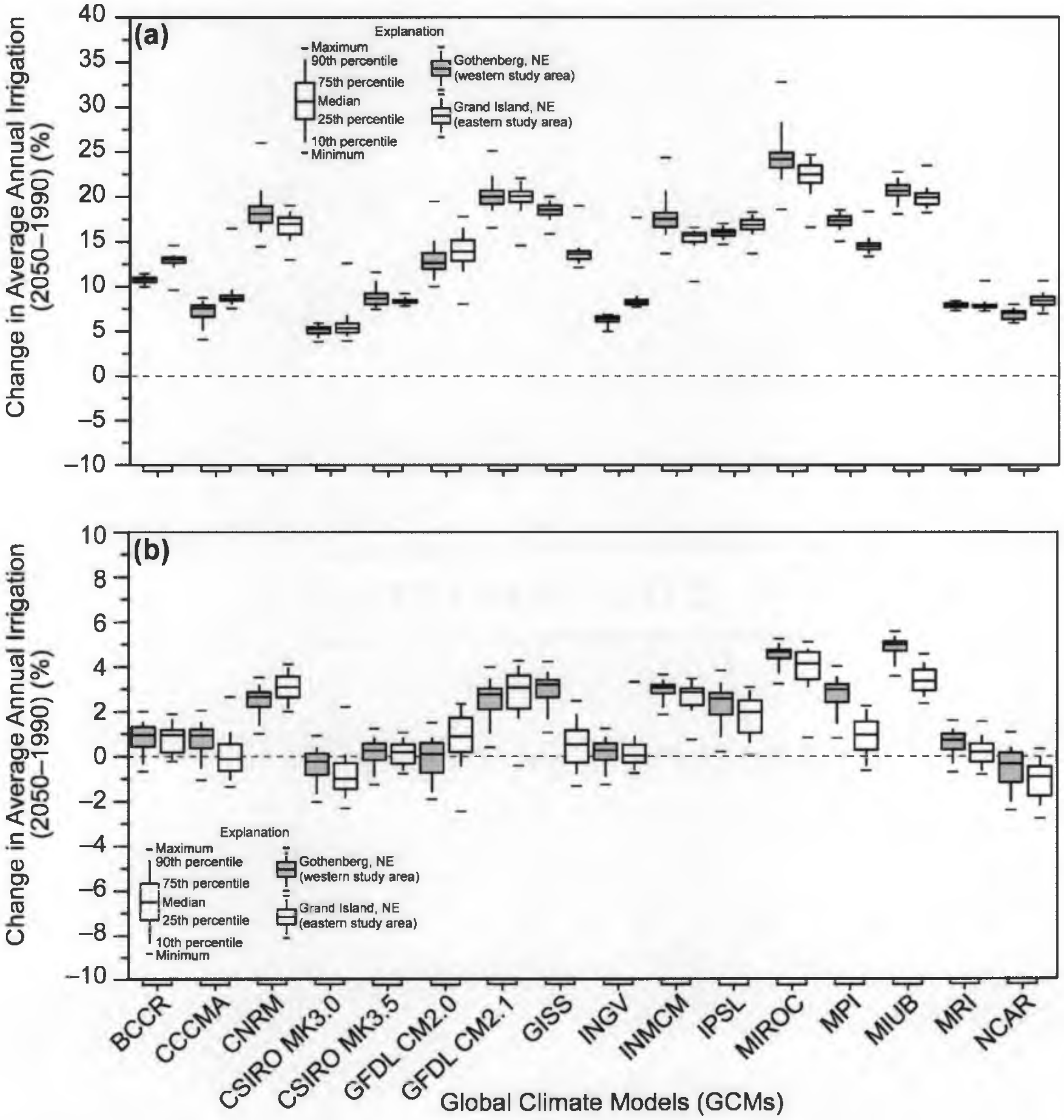

Appendix 2: Boxplots of the percent (%) change in simulated average annual irrigation between 2050 and 1990 at Gothenburg, Nebraska (western study area) and Grand Island, Nebraska (eastern study area) for (a) high global warming scenario (+2.4°C, 567 ppm CO2) and (b) low global warming scenario (+1.0°C, 478 ppm CO2) from 16 global climate models (GCMs). Each boxplot represents 30 years of simulated precipitation. The dashed line represents no change; positive values indicate greater future average annual precipitation and negative values indicate smaller future average annual precipitation. Note the different y-axis scales.

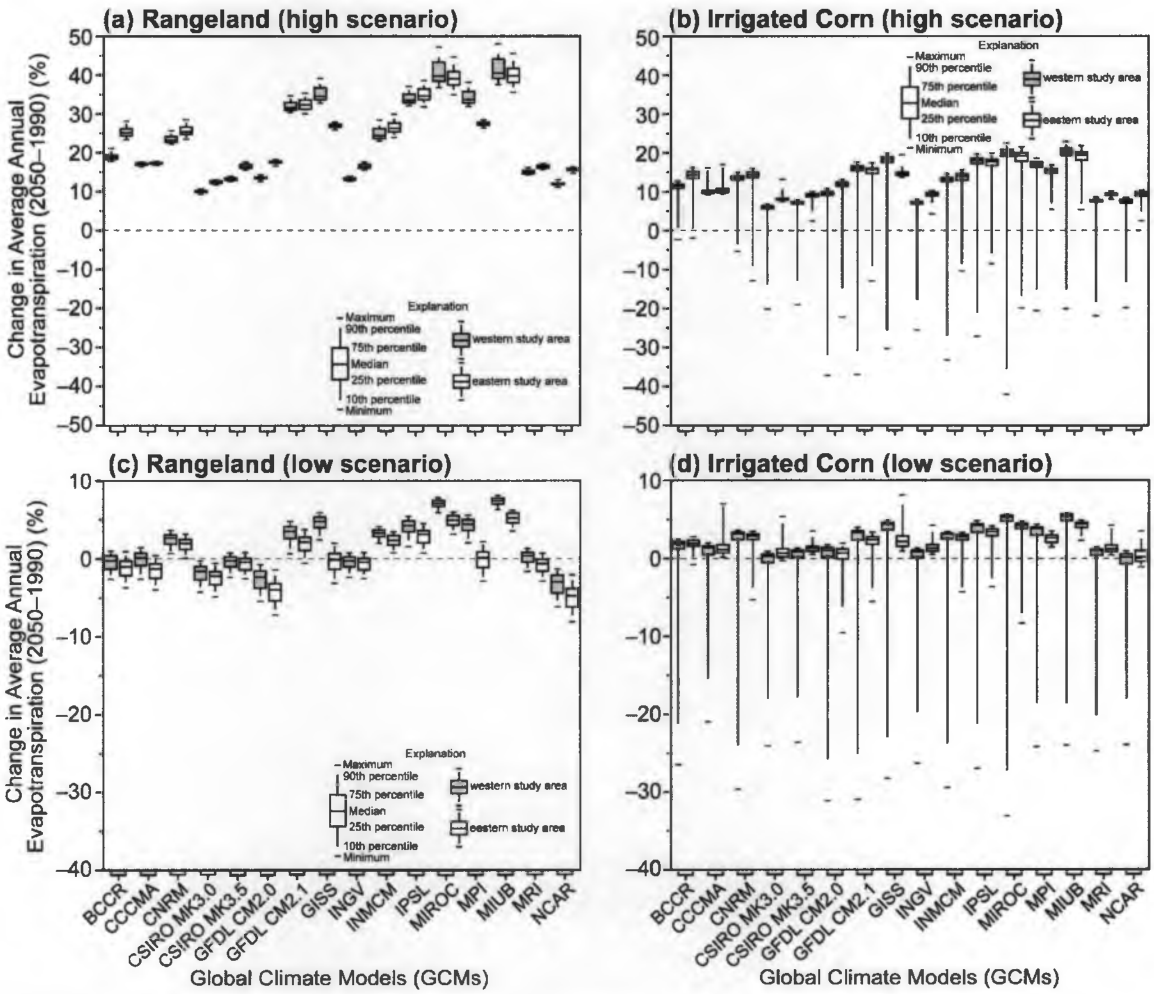

Appendix 3: Boxplots of the percent (%) change in simulated average annual evapotranspiration between 2050 and 1990 at Gothenburg, Nebraska (western study area) and Grand Island, Nebraska (eastern study area) for (a) high global warming scenario (+2.4°C, 567 ppm CO_2) and (b) low global warming scenario (+1.0°C, 478 ppm CO_2) from 16 global climate models (GCMs). Each boxplot represents 30 years of simulated precipitation. The dashed line represents no change; positive values indicate greater future average annual precipitation and negative values indicate smaller future average annual precipitation. Note the different y-axis scales.

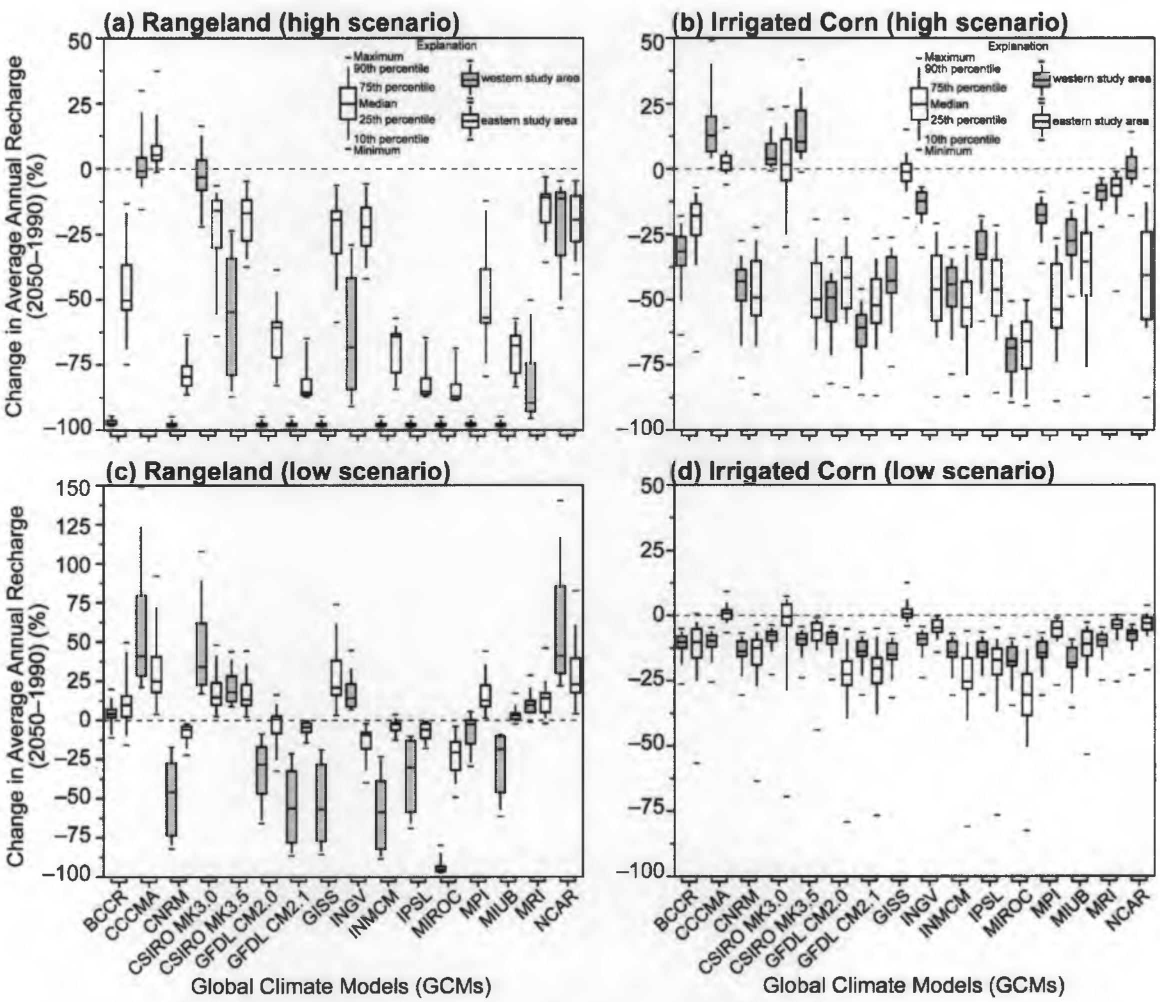

Appendix 4: Boxplots of the percent (%) change in simulated average annual recharge between 2050 and 1990 at the western and eastern study area sites beneath (a,c) rangeland and (b,d) irrigated corn for (a,b) high global warming scenario (+2.4°C, 567 ppm CO_2) and (c,d) low global warming scenario (+1.0°C, 478 ppm CO_2) from 16 global climate models (GCMs). Each boxplot represents 30 years of simulated recharge. The dashed line represents no change; positive values indicate greater future average annual precipitation and negative values indicate smaller future average annual precipitation. Note the different y-axis scales for (c) rangeland (low scenario).